

Study on a Mesoscale Convective Vortex Causing Heavy Rainfall during the Mei-yu Season in 2003

SUN Jianhua^{*1,2} (孙建华), ZHAO Sixiong¹ (赵思雄), XU Guangkuo¹ (徐广阔), and MENG Qingtao¹ (孟庆涛)

¹*Institute of Atmospheric Physics, Chinese Academy of Sciences, Beijing 100029*

²*State Key Laboratory of Severe Weather, Chinese Academy of Meteorological Sciences 100084*

(Received 8 September 2009; revised 12 November 2009)

ABSTRACT

The strong heavy rainfall on 3–5 July 2003 causing the severe flooding in Huaihe River basin (HRB), China is studied. It is noted that there are sometimes mesoscale convective vortex (MCV) in East Asia during the mei-yu season. Simulation results from the ARPS (Advanced Regional Prediction) data analysis system (ADAS) and WRF model were used to study the development of the mesoscale convective system (MCS) and mesoscale convective vortex (MCV). It is confirmed that the MCV formed during the development of a previous severe MCS. A closed vortex circulation can be found below 600 hPa with a vorticity maximum in the middle troposphere. The evolution process of the MCV can be divided into three stages: initiation, maturation, and dissipation. During the mature stage of the MCV, a downdraft occurred in the center of the MCV and new convection developed in southeast of the MCV. The convergence and the tilting in the lower troposphere convergence and vertical advection in the middle troposphere were the main vorticity sources in the MCV initiation stage. Finally, a conceptual model between the mei-yu front and the embedded MCS and MCV is proposed. The mei-yu front was the background condition for the development of the MCS and MCV. A low level jet (LLJ) transported moisture and the weak cold air invasion via a trough aloft in the middle troposphere and triggering the severe convection. Furthermore, the intensified jet was able to result in the initiation of new “secondary” areas of convection in the eastern part of the MCV.

Key words: mesoscale convective system, mesoscale convective vortex, doppler radar, WRF model

Citation: Sun, J. H., S. X. Zhao, G. K. Xu, and Q. T. Meng, 2010: Study on a mesoscale convective vortex causing heavy rainfall during the mei-yu season in 2003. *Adv. Atmos. Sci.*, **27**(5), 1193–1209, doi: 10.1007/s00376-009-9156-6.

1. Introduction

China is located in the East Asia Monsoon Area. During the summer monsoon season, there is a quasi-stationary front with intense rainfall called the mei-yu front (MYF) in China (Baiu front in Japan), which appears very often as a long cloud band extending from China to the northwestern Pacific through the Japanese Islands, and occurring from the middle June to middle July (Tao, 1980). Its strong activity sometimes induces floods in the Yangtze River basin (YRB) and Huaihe River basin (HRB). The geographic regions of the YRB and HRB are shown in Fig. 1a. Previous studies over the past several decades related to MYF activity can be summarized as follows: (1) The MYF corresponds to a quasi-stationary cloud zone

located along the northern periphery of the Western Pacific Subtropical High (WPSH), and is characterized by small temperature gradient and large moist gradients over China, though the temperature gradient which is more dominant over Japan (Kato, 1985; Ninomiya and Muraki, 1986); (2) The MYF is associated with a strong southwesterly pattern known as a low-level jet (LLJ), which transports a large amount of moisture to the MYF, and generates not only moisture gradients but also a thick, moist, neutral stratification (Ninomiya and Kiyama, 1974; Tao, 1980); (3) Many mesoscale convective systems and mesoscale disturbances which move eastward along the front as the main makers of heavy rains are embedded in the MYF (Ding, 1993; Ninomiya, 2000).

Given severe flooding of the HRB in 1991 and

* Corresponding author: SUN Jianhua, sjh@mail.iap.ac.cn

the YRB in 1998, many studies have focused on the heavy rainfall producing systems, e.g., mesoscale convective systems and vortices (Ding, 1993; Zhao et al., 2004), because the mei-yu front heavy rainfalls were directly caused by such mesoscale systems. Ding (1993) pointed out that the heavy rainfalls over HRB in 1991 were related closely with the meso- β scale system originated from shear lines or the mei-yu front. The heavy rainfall with flooding over the YRB in 1998 was produced by MCSs especially, and the severe heavy rainfall in Wuhan and Huangshi cities, Hubei Province, China, on 20–22 July 1998 were brought about by M β CS (Bei et al., 2002). Zhao et al. (2004) have studied the structure of the mei-yu front, the formation and development of mesoscale vortices, and the characteristics of mesoscale rain clusters in the cases in July 1998. On the basis of the analysis of intensive observational data from the China Heavy Rain Experiment and Study (CHeRES), a multi-scale conceptual model of heavy rainfall in the mei-yu front was proposed

(Sun et al., 2005). It is noted that the outflow in the boundary of the convection line may trigger new a convection line and that these convection lines usually move along with mesoscale surface convergence lines.

Since 2000, and especially in 2003 and 2007, heavy rainfall causing severe floods has occurred in the HRB, rather than the YRB. The mei-yu season began on 21 June and ended on 12 July 2003 (Zhang et al., 2004), and the heavy rainfall period could be divided into two stages: a first one of 21–28 June with rainbands located in the YRB, and a second one of 29 June–11 July with rainbands located in the HRB. The accumulated precipitation of the mei-yu season over the HRB, totaled above 600 mm, reached 400 mm during the second stage, and resulted in severe flooding over the HRB. It has been noticed that three heavy rainfall processes occurred during the second stage of that year's mei-yu, namely, 29 June–1 July, 3–5 July, and 8–11 July. The most severe one among these rainfall cases occurred during 3–5 July, in which severe heavy rainfall covered a wide area including Henan, Anhui, and Jiangsu Provinces. The precipitation totals in Chuzhou ($32^{\circ}18'N$, $118^{\circ}18'E$, Fig. 1b), Anhui Province and Nanjing ($32^{\circ}00'N$, $118^{\circ}48'E$, Fig. 1b), Jiangsu Province were 380 and 195 mm, respectively, results which were caused mainly by mesoscale convective systems and mesoscale vortices in the mei-yu front. Essentially, predictions of mei-yu front rainbands are generally successful; however, the maxima of heavy rainfalls cannot be predicted well sometimes. The reason is that these maxima are associated with the formation and development of mesoscale vortex (disturbances), and the mechanisms governing them has not yet been revealed from the point of view of mesoscale dynamics. Moreover, although mesoscale convective systems (MCSs) have been somewhat studied during past decade, the details of mesoscale convective vortexes (MCVs) have only been paid more attention relatively recently. In the heavy rainfall case of 3–5 July 2003, not only were heavy rainfall and floods caused over HRB, but also MCSs and a MCV were reported. Therefore, it is an opportunity for the analysis to highlight this, so as to better understand the development of mesoscale convective systems and improve their prediction.

It has been found that there exist some MCVs in the rainy season in North America. An important impact is that an MCV can cause a secondary convection in the area nearby. Undoubtedly, they are very meaningful for precipitation prediction. Some scientists have been investigating this aspect. Observations (Smull and Houze, 1985; Leary and Rappaport, 1987; Johnson et al., 1989; Jorgensen and Smull, 1993) and numerical simulations (Zhang and Fritsch, 1988a, b)

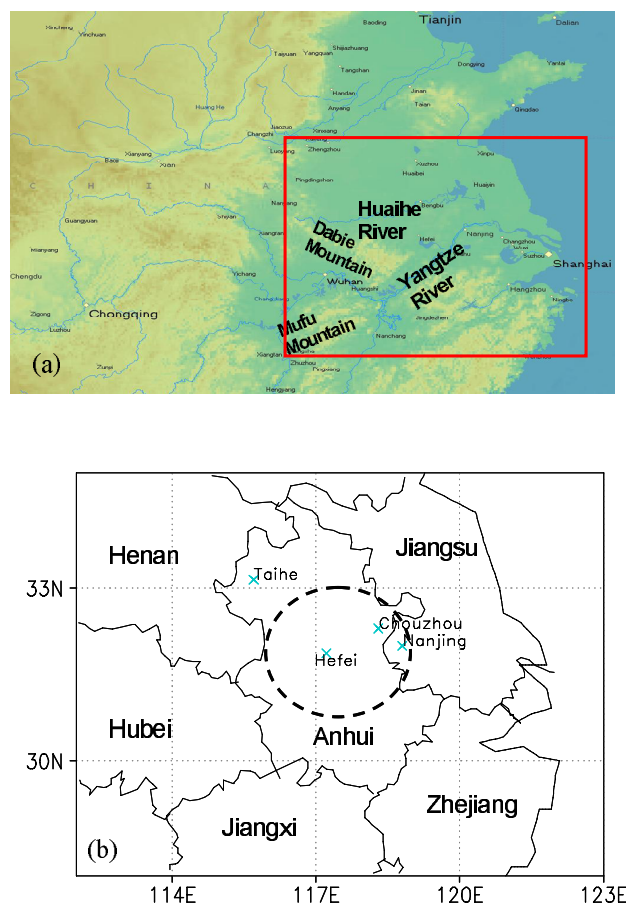


Fig. 1. (a) Orography around the Yangtze River and Huaihe River basins, (b) districts under study indicated by the red rectangle. The bold circle represents the observation area of the Doppler radar in Hefei.

have shown that a cyclonic circulation is generated within the stratiform precipitation region of convective complexes. The first observational evidence of residual cyclonic circulations was provided by Johnston (1981), who identified a number of circulations in film loops of visible satellite imagery. The horizontal scales of MCVs are as large as several hundred kilometers and time scales range from hours to days. Various studies have shown that an MCV can form in a variety of ways. MCVs are the class of larger mesoscale vortices with 100–300 km diameter that can organize moist convection. These vortices are several kilometers deep and sometimes span most of the troposphere (Fritsch et al., 1994; Davis and Trier, 2007). From a vorticity dynamics perspective, the MCV is often viewed as resulting from the convergence of synoptic-scale vorticity, with the largest contribution coming from earth's rotation (Bartels and Maddox, 1991; Skamarock et al., 1994).

Features of the large-scale environment that appear conducive to the formation and longevity of MCVs include weak flow, weak vertical shear, weak background relative vorticity, and intense horizontal and vertical moisture gradients (Bartels and Maddox, 1991)). And the rapid mesovortex generation observed can be explained by the stretching term of the vorticity equation. Systematic study of convectively generated vortices with cloud-resolving numerical models (Weisman and Davis, 1998) has illustrated that the long-lived vortices, comparable in horizontal scale to that of the MCSs from which they are spawned (termed system-scale vortices), are favored when weak-to-moderate environmental vertical shear is confined to the lower troposphere. It should be noticed that in North America, a scientific project “the Bow Echo and Mesoscale Convective Vortex Experiment (BAMEX)” has been conducted between 20 May and 6 June 2003. In the BAMEX, two types of systems were emphasized: one producing severe surface wind (bow echo) and the other producing long-lived mesoscale convective vortices (MCVs) capable of initiating subsequent convection (Davis et al., 2004). In China, the research on MCVs has just started recently.

In the present paper, the scientific problems are: Do there exist MCVs in East Asia during the mei-yu season? If so, what are the characteristics of the evolution and structure? What are the impacts on heavy rainfall? Are the main characteristics of MCVs in East Asia reproducible by a mesoscale numerical model? In order to clarify the formation of MCVs along mei-yu front, MCSs and MCVs during the heavy rainfall case of 3–5 July 2003 are investigated. The data and method utilized in this study are introduced in section 2. In section 3, synoptic conditions of the heavy rainfall process are described. The MCS/MCV pro-

ducing the most severe heavy rainfall at Chuzhou and Nanjing and their developing conditions are diagnosed. The numerical model, experimental design, and verification of rainfall predictions with observations are given in section 4. The formation and structure of MCVs are discussed in section 5. Finally, the conclusions and discussions are presented in section 6.

2. Data and methodology

Infrared TBB (Black Body Temperature) data from Geostationary Operational Environmental Satellite (GOES9) have been used to analyze the activities of MCSs and MCVs along the mei-yu Front in July 2003. The hourly data were available and cover the East Asia area (20° – 70° N, 70° – 160° E). The spatial resolution of TBB data was 0.05° . The 24-hour and hourly precipitation amounts in China were provided by China Meteorological Administration (CMA) and have also been utilized. The synoptic setting was conducive to MCS and MCV occurrence as revealed by using the NCEP (National Center for Environmental Prediction, US) analysis grid $1^{\circ} \times 1^{\circ}$ data. The rawinsonde data were analyzed for the cases to investigate and to examine the evolution of the large-scale thermodynamic and kinematic fields.

In order to get high-resolution data to understand development of MCVs, the simulated output by the WRF model was employed to investigate the process. NCEP analysis grid $1^{\circ} \times 1^{\circ}$ data was used as background data. To improve the simulation of MCSs and MCVs, the surface, rawinsonde data, and Hefei Doppler data were also used to obtain the initial fields.

3. Synoptic settings and development of MCS/MCV

3.1 Synoptic conditions of the heavy rainfall process

Besides the strong intensity of the heavy rainstorm in the HRB from 3 to 5 July 2003, another important reason which contributed to the severe flooding was that the rainstorm moved from upper to lower reaches of the HRB. From 0000 UTC 3 to 0000 UTC 4 July, a rain belt of width 200 km extended from Henan Province to the northern part of Anhui Province and Jiangsu Province, of which the center of the heavy rainstorm, covering an area of about $300 \text{ km} \times 100 \text{ km}$, was located in the central Henan Province and northern Anhui Province (Fig. 2a). On 4 July, the rainband moved southeastward by about 200–300 km, the main heavy rainfall was in the central and southern part of Jiangsu Province and the heaviest rainstorm area was near the border between Anhui Province and Jiangsu

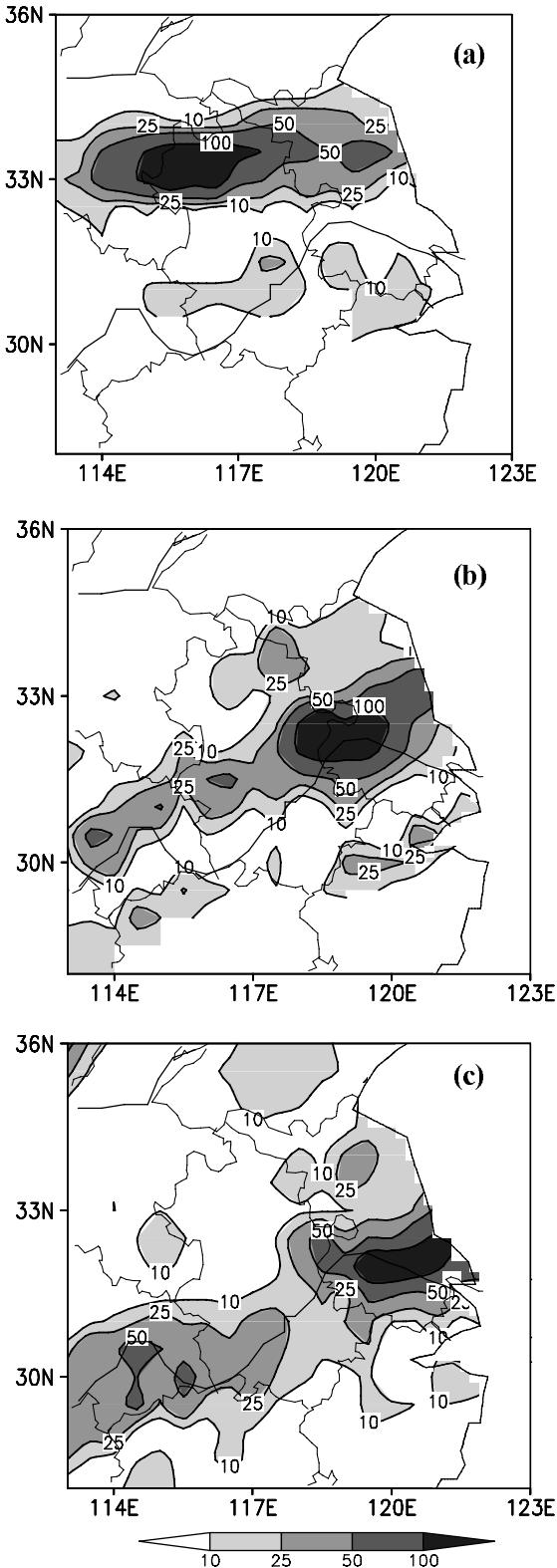


Fig. 2. The daily precipitation amounts for 3–5 July 2003 (units: mm): (a) 0000 UTC 3 to 0000 UTC 4 July; (b) 0000 UTC 4 to 0000 UTC 5 July; (c) 0000 UTC 5 to 0000 UTC 6 July.

Province (Fig. 2b). On 5 July, the rainstorm was located in the southern part of Jiangsu Province (Fig. 2c). The above-mentioned analysis demonstrated that widespread heavy rainfall from 3 to 5 July happened firstly in the upper reaches and moved gradually to the lower reaches of the HRB. If this kind of moving severe precipitation merged with the flood peak from the upper reaches, the existing high water levels in the middle and lower reaches rose very rapidly and the flood situation became even worse.

The occurrence of this kind of heavy rainfall was highly associated with the synoptic circulations. The western Pacific subtropical high (WPSH) at 500 hPa extended to west of 110°E from 3 to 5 July and it retreated southeastward gradually to 120°E on 6 July. In the middle latitude area, a trough propagated eastwards from 3 to 6 July. The Henan and Anhui Provinces, located in HRB, were located ahead of the trough and the south flank of the upper level westerly jet from 4 to 5 July (Figs. 3a, b). In addition, a relatively strong southwest low level jet (LLJ) with maximum of 15–18 m s⁻¹ formed to the northwest of the WPSH in the lower troposphere (Figs. 3c, d). From 3 to 5 July, the maxima of the heavy rainfall were maintained to the northern flank of the center of the LLJ. A northeast-southwest oriented shear-line along north rim of the WPSH formed on 4 July (Fig. 3c). The east part of the shear-line was a shear between southwesterly and northeasterly on 5 July (Fig. 3d), in which the weak cold air was active. Therefore, the rainfall on 5 July was relatively lighter than that on 4 July (Fig. 2). During this event, the large-scale circulation was advantageous for the formation and development of the convection systems in the mei-yu front, and the eastward propagating of the trough aloft caused the movement of the rainy areas.

3.2 The activities of MCS/MCV during the heavy rainfall

The convection during this event was very active. The development of MCSs in Henan Province and the northern part of Anhui Province caused the continuous heavy rainfall on 3 July (Fig. 2a). After 0700 UTC 4 July, the convection in the central and northern part of Anhui Province began to be active, and the main formation area of the convection was located in the Dabie Mountains and the YRB among the Dabie and Mufu Mountains on 4–5 July (Fig. 4). The location of the mountains and the YRB are shown in Fig. 1. The convection, occurred in the central part of Anhui Province at 1200 UTC 4 July, and formed a meso- α cloud cluster covering an area of about 1000 km × 500 km at 2000 UTC 4 July, which was the biggest MCS during this heavy rainfall. The development of

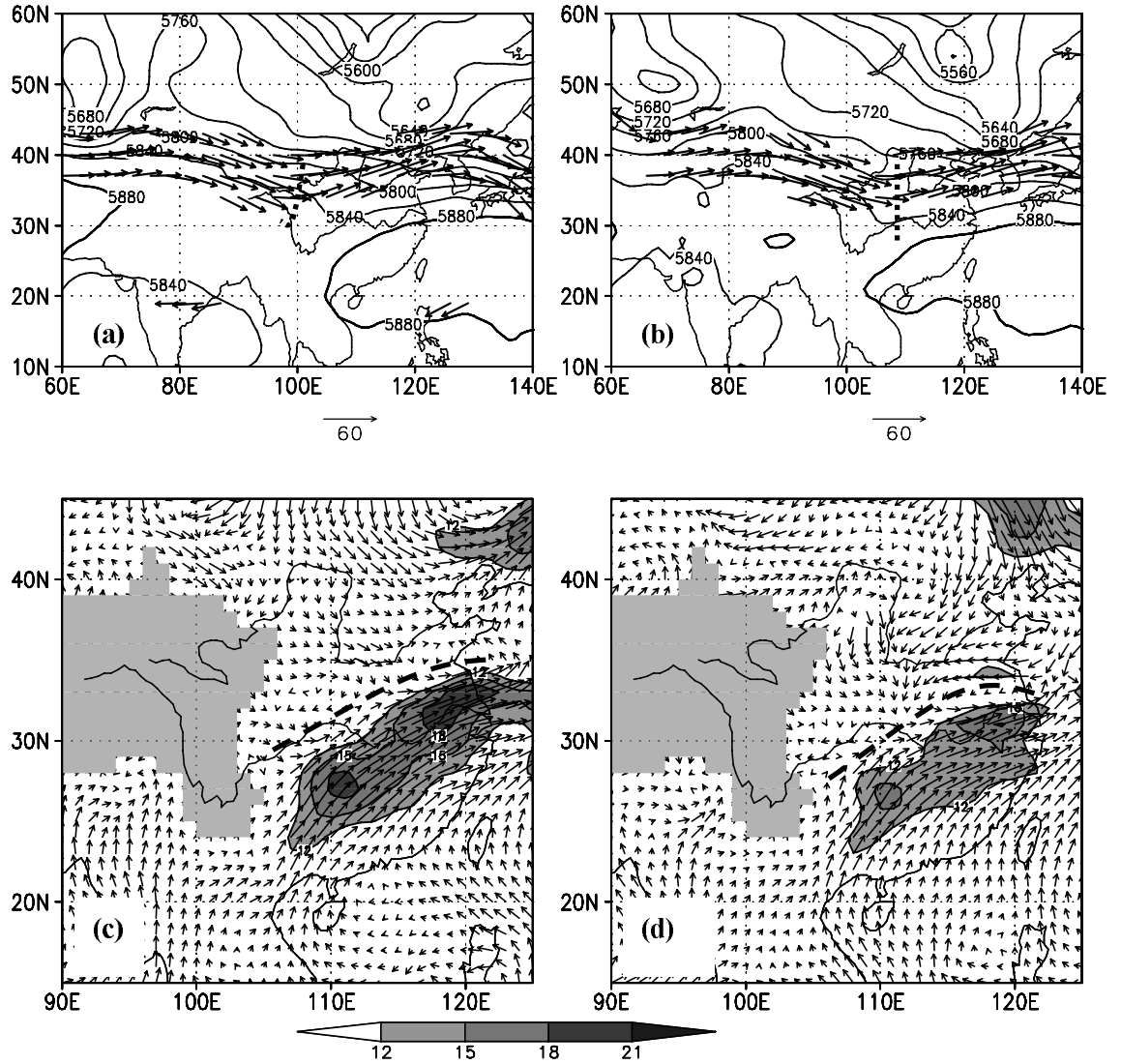


Fig. 3. The geopotential height at 500 hPa (gpm) and wind speed greater than 30 m s^{-1} at 200 hPa (vector, upper panel), and wind vector and Low Level Jet ($\text{LLJ} > 12 \text{ m s}^{-1}$) at 850 hPa (lower panel), from 0000 UTC 4 to 5 July 2003. The bold dashed line represents the trough line in (a) and (b), and the boldface dashed lines are shear lines, with light shading showing topography higher than 1500 m and dark shading for wind speeds larger than 12 m s^{-1} in (c) and (d).

the system caused heavy rainfall with 45 mm h^{-1} at 1600 UTC 4 July (Fig. 4). A vortex was located to the north of 35°N and a convergence zone with severe precipitation appeared to the south of the vortex at 1800 UTC 4 July. The convection in the cloud cluster weakened after 0000 UTC 5 July (Fig. 4), and a new vortex developed over the HRB (Fig. 5b). The severe precipitation occurred prior to the appearance of vortex. During the initial stage of the vortex, the convection and precipitation got weaker (Fig. 4 and Fig. 5c). After 0600 UTC 5 July, the cloud system of vortex moved eastward (Fig. 4 and Fig. 5d). However, after the initiation of the MCV, convection developed again in the southern part of Anhui Province

and Jiangsu Province, which indicated new convection; that is, a secondary convection was apparently initiated by the MCV. It has been emphasized that an important aspect of MCVs is this subsequent convective development within long-lived discontinuous heavy precipitation episodes. Subsequent deep convection was observed in the vicinity of MCVs in slightly greater than 1/2 of the MCV cases (Trier et al., 2000). Although a statistical study of MCVs in China has not yet been conducted, Chinese Meteorologists have always focused on the fact that such vortices may produce heavy rainfall along the mei-yu front (Zhao et al., 2004; Sun et al., 2004). Meanwhile, in fact, the “secondary convection” and precipitation caused by the

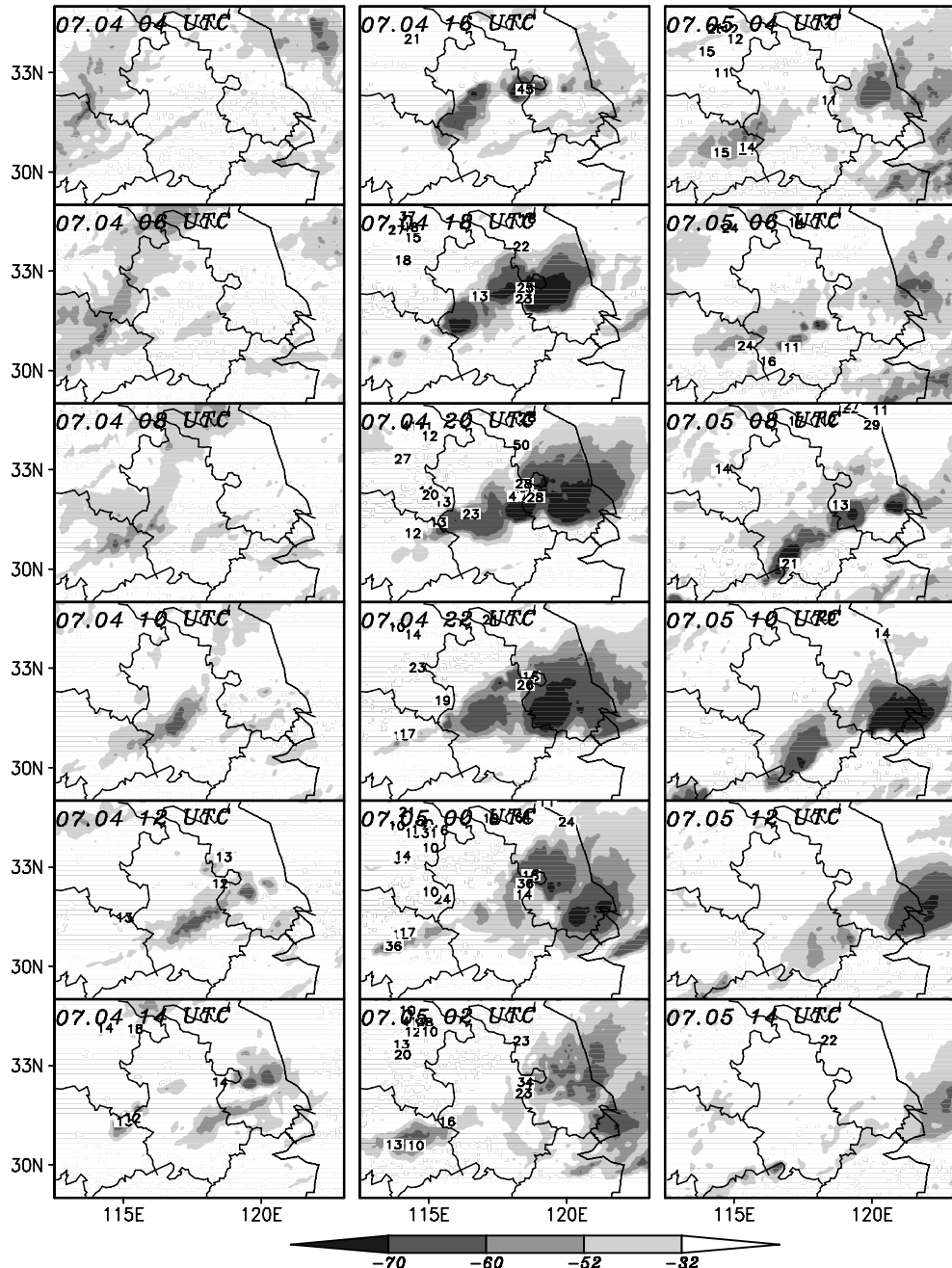


Fig. 4. The infrared brightness temperature in $^{\circ}\text{C}$ from GOES-9 at 0400 UTC 4 to 1400 UTC 5 July 2003. The number is hourly precipitation amount larger than 10 mm h^{-1} .

mosescale vortices has been revealed in China (Zhao et al., 2004), even though the mechanism of the “secondary convection” caused by MCVs in the mei-yu front could differ from cases in North America because China belongs the monsoon area.

To summarize, a series of MCSs were triggered over this area, which resulted in the heavy rainfall from 3 to 5 July. A vortex formed when the meso- α MCS developed to the mature stage and the vortex resulted from the convection development. The detailed evo-

lution and structure of MCV will be investigated by simulation in section 5.

3.3 The synoptic conditions for developing of MCSs and MCV

The synoptic circulations and MCSs for the occurrence of the strong heavy rainfall in Anhui and Jiangsu Provinces from 4 to 5 July were analyzed in this section. Here the observations from sounding stations in Nanjing were chosen to research the stratification evo-

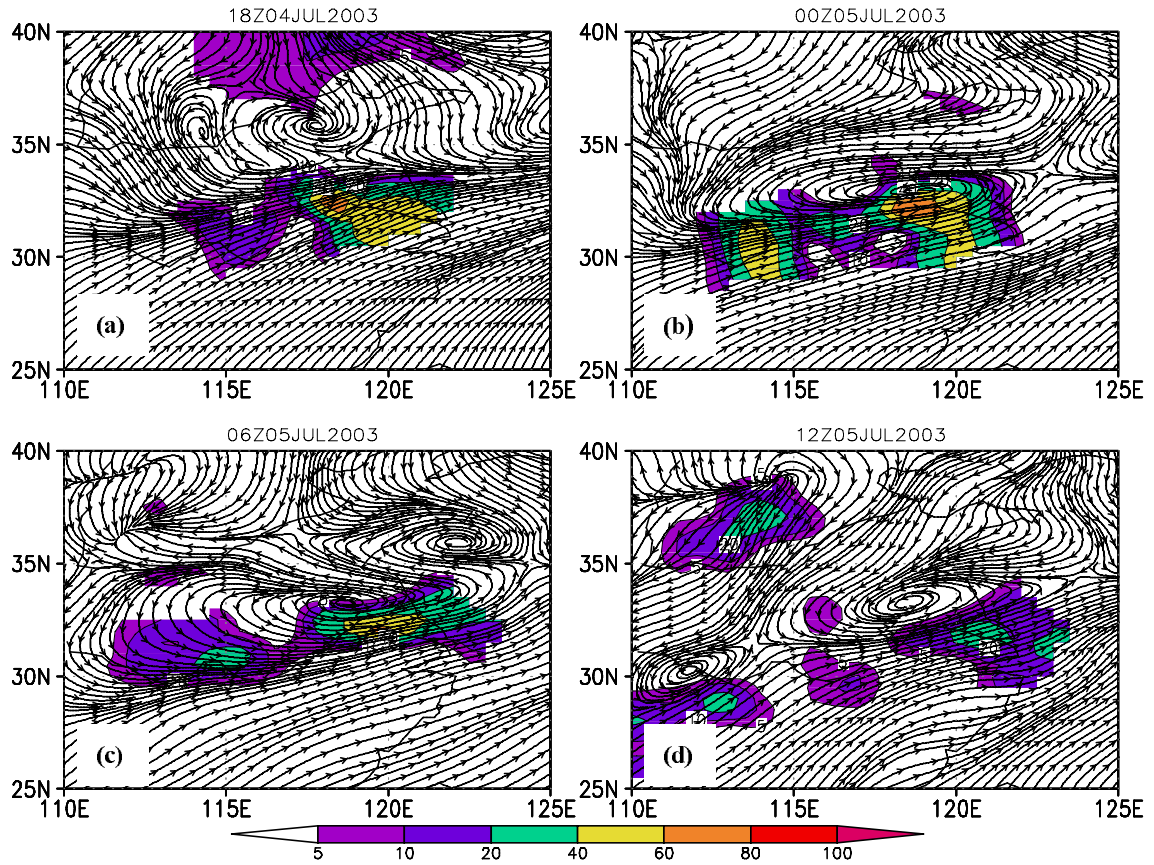


Fig. 5. The streamlines at 850 hPa from 1800 UTC 4 July to 1200 UTC 5 July. The shadings are 6-hourly precipitation (units: mm): (a) from 1200 UTC–1800 UTC 4 July, (b) from 1800 UTC 4 July–0000 UTC 5 July, (c) from 0000 UTC–0600 UTC 5 July, (d) from 0600 UTC–1200 UTC 5 July.

lution of MCV development. The parameters calculated by the sounding data from 0000 UTC 4 to 1200 UTC 5 July are shown in Table 1. Figure 6 shows the evolution of wind, relative humidity, and pseudo-equivalent potential temperature (θ_{se}) from 2 to 5 July 2003.

At 0000 UTC 4 July, relative humidity for whole layers were less than 70% (Fig. 6a), with precipitable water of 45.7 mm and Convective Available Potential Energy (CAPE) of 1029 J kg^{-1} (Table 1). Thus, the convection instability was significant (Fig. 6b). At 1200 UTC 4 July, CAPE increased to 1565 J kg^{-1} , while the precipitable water was only 56.6 mm. The

vertical shear was $3.35 \times 10^{-3} \text{ s}^{-1}$ in lower troposphere and $1.23 \times 10^{-3} \text{ s}^{-1}$ in middle troposphere. Prior to the occurrence of rainfall, the dry layer in the middle troposphere might have been related to the dry intrusion accompanying the northern air flow behind the trough aloft. The dry intrusion at middle levels enhanced the convection instability in the lower troposphere. Furthermore, the southwesterly wind at low levels intensified to 20 m s^{-1} at 0000 UTC 4 July (Fig. 6a), which means that the moisture transportation at low levels by the LLJ increased the moisture content and enhanced the CAPE from 0000 UTC to 1200 UTC 4 July. At 1200 UTC 4 July, the K index

Table 1. The physical quantities calculated by upper air sounding data at Nanjing stations from 0000 UTC 4 to 1200 UTC 5 July 2003.

Time	Variables						
	CAPE (J kg^{-1})	CIN (J kg^{-1})	LI	K	PWAT (mm)	Shear at 700–925 hPa (10^{-3} s^{-1})	Shear at 300–700 hPa (10^{-3} s^{-1})
0000 UTC 4 July	1029	36	-6	33	45.7	2.16	1.55
1200 UTC 4 July	1565	19	-5	40	56.6	3.35	1.23
0000 UTC 5 July	563	15	-2	39	67.2	6.03	1.51
1200 UTC 5 July	620	20	-2	35	59.6	7.87	1.30

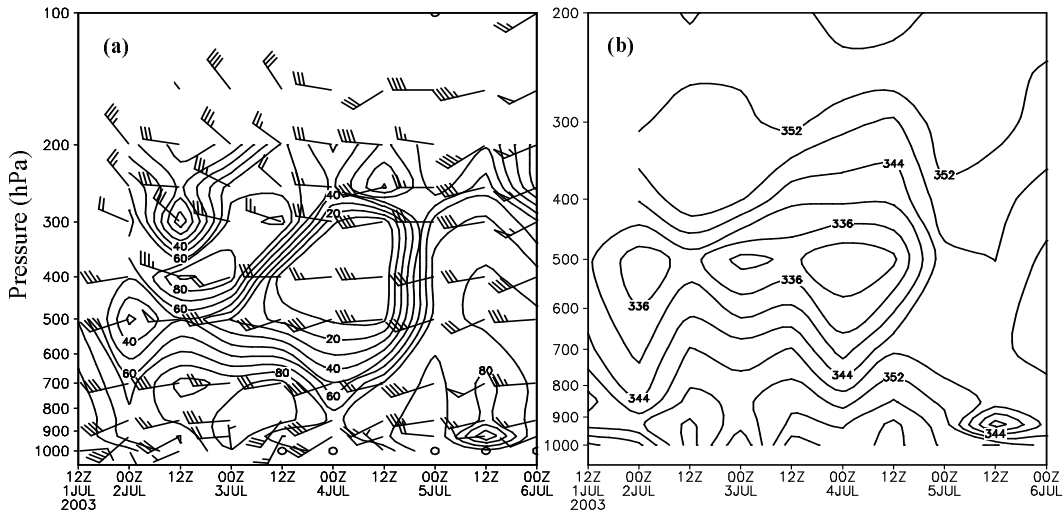


Fig. 6. The wind vector (full bar, 4 m s^{-1} , flag, 20 m s^{-1}), relative humidity (%) (a) and θ_{se} (b, units: K) at Nanjing from 2 to 6 July 2003.

and the lifting index (LI) were 40 and -5 , respectively, which indicated that the atmosphere had been very unstable. At this time, the convective inhibition energy (CIN) at Nanjing was only 19 J kg^{-1} . If some kind of triggering mechanism existed, CAPE could be released very easily, which would induce strong upward motion in Nanjing. Actually, the convection began to develop quickly after 1200 UTC 4 July. This indicated that the mesoscale environment conditions regarding thermodynamic instability and vertical shear between East Asia and North America are quite similar to each other, even though the synoptic environment between both of them was quite different.

At 0000 UTC 5 July, severe heavy rainfall had already occurred in Nanjing, while the whole layer became quite moist (Fig. 6a). The relative humidity below 300 hPa exceeded 75%. The CAPE in Nanjing decreased and was 563 J kg^{-1} at this time, which revealed that most of the CAPE had been released. The rainfall lasted until 0600 UTC 5 July, and the precipitation amount in about two hours exceeded 20 mm (not shown). Furthermore, as it is shown from the evolution of the wind speed at low levels in Nanjing, the LLJ always existed at 900–500 hPa. The intensity of the LLJ streak was usually more than 15 m s^{-1} , and the LLJ appeared before the rainfall on 4–5 July. However, there was a deep convection instability layer on 4 July, while there was a neutral layer in the afternoon of 5 July (Fig. 6b). This neutral layer on 5 July resulted from the heavy rainfall. The vertical shear was $6.03 \times 10^{-3} \text{ s}^{-1}$ in lower troposphere and $1.51 \times 10^{-3} \text{ s}^{-1}$ in middle troposphere, which was relatively larger at 0000 UTC 5 July than at 1200 UTC 4 July. The MCV formed just at that time. The mentioned-above values of CAPE, LI, CIN, and vertical shear in East

Asia are basically equivalent to those in North America. The values seem to be reasonable and explainable (Trier et al., 2000).

4. Experimental scheme of numerical simulation and the verification

4.1 Model description and experimental schemes

As is well-known, the numerical prediction of severe convective systems is difficult, and is very sensitive to the initial conditions of model. For a better description of the structure and evolution of MCS, Doppler Radar data has been collected because the radar data has higher spatial and temporal resolution and can be used to observe more mesoscale information. In the present study, we adopt a simpler method to assimilate Chinese Doppler radar data. Here, the ARPS data analysis system (ADAS) system (Zhang, 1999; Xue et al., 2003) was employed to form initial conditions for the Weather Research and Forecasting (WRF) model. The WRF model is a next generation mesoscale modeling system designed to replace existing U.S. research and operational models (Skamarock et al., 2005). Based on the simulation, the output is utilized to diagnose the evolution and development of MCSs and MCVs because there are few intensive observational data available.

Four experiments are designed as listed in Table 2. The radar data was obtained from the Doppler radar in Hefei (Fig. 1). The background of the initial conditions was obtained from NCEP (National Center for Environmental Prediction, US) operational model analyses at resolution of $1^\circ \times 1^\circ$. On the basis of the

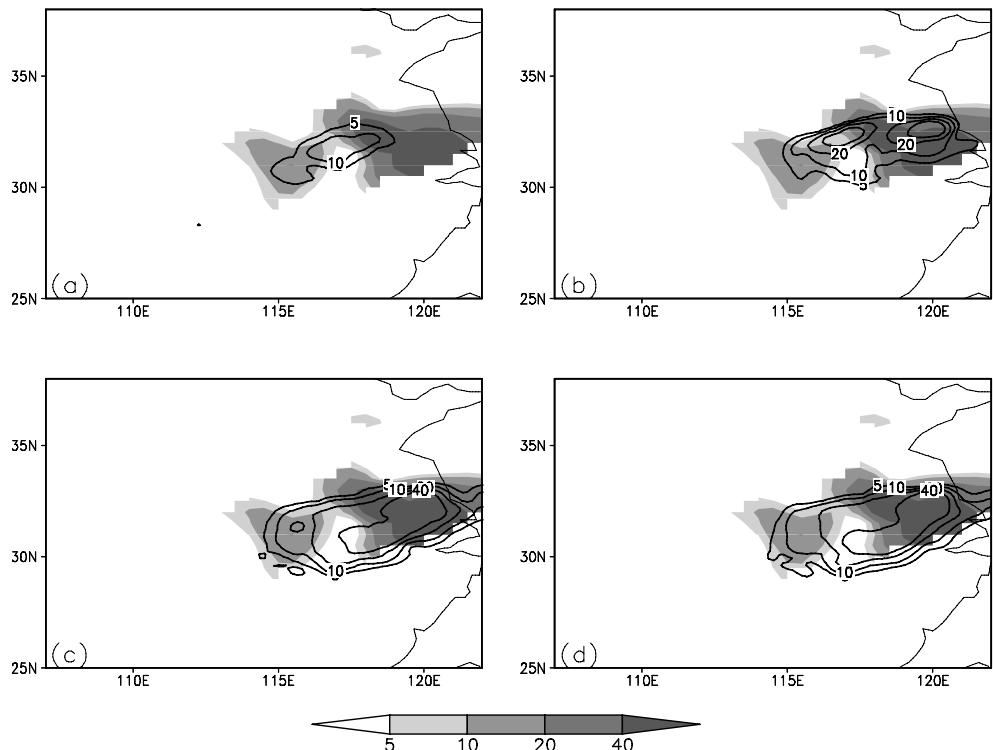


Fig. 7. The simulated precipitation amount (solid line) and observations (shaded) from 1200 UTC to 1800 UTC on 4 July 2003 (units: mm): (a) Expt. CNTL; (b) Expt. RADAR-V; (c) Expt. RADAR-R and (d) Expt. RADAR-RV.

background, the initial field of Expt. CNTL only used conventional surface and sounding data by ADAS. Except for routine data, in Expt. RADAR-V and Expt. RADAR-R radial velocity and radar reflectivity are used, respectively. And both radar reflectivity and radial velocity were applied in Expt. RADAR-RV. The simulation domain covers East Asia, centered at 31.0°N, 112.0°E. Three domains with horizontal resolution of 36 km, 12 km, and 4 km are configured with one-way simulation, respectively. The three domains have grid points of 101×101, 129×119, and 161×161. The model top is located at 50 hPa and there are 31 sigma levels in the vertical. The modeling system employs the Yonsei University (YSU) PBL scheme (Noh et al., 2003), the Noah land surface model (Chen and Dudhia, 2001), a long wave and short-wave radiation parameterization (Dudhia, 1989), and a bulk microphysics parameterization based on Lin et al. (1983). Kain-Fritsch cumulus parameterization (Kain and Fritsch, 1992, 1998) is used in domains one and

two, and no cumulus parameterization is used in domain three. The WRF model is initialized at 1200 UTC 4 July and integrated for the 24-h period over the three domains.

4.2 The verification of simulated precipitation with observations

As the resolution of the observational data is relatively low, and it cannot be compared with the simulation results of the fine-mesh grid, the simulated precipitation in domain one with 36 km grid distance is verified with the observational precipitation.

The precipitation amount and rainfall area of the first 6 hours in Expt. CNTL differs greatly from the observations (Fig. 7a), the rainfall area is apparently relatively small and the precipitation amount is relatively weak. This can be understood as being caused not only by spin up of the numerical model, but also by the quantity of the data involved. With the adoption of the radar data in the three experiments (Figs.

Table 2. A list of the experiments with different initial conditions.

	CNTL	RADAR-V	RADAR-R	RADAR-RV
Routine data	Yes	Yes	Yes	Yes
Radar radial velocity	No	Yes	No	Yes
Radar reflectivity	No	No	Yes	Yes

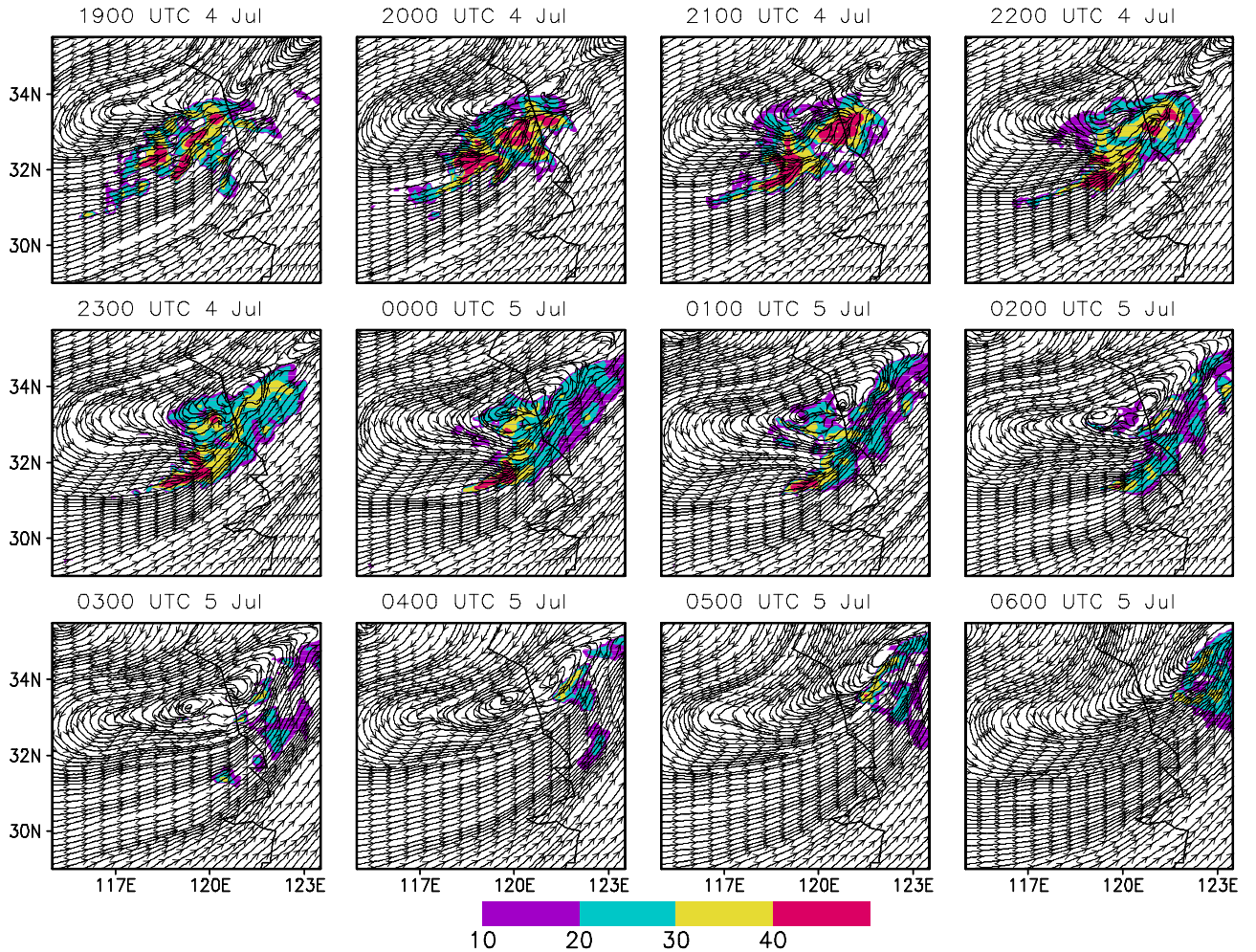


Fig. 8. The simulated circulation at 700 hPa and retrieved radar reflectivity (shaded, dBZ) from 1900 UTC 4 July to 0600 UTC 5 July.

7b–d), the simulated results improved over that of Expt. CNTL. The simulated precipitation of these three experiments are much like the observations, and they simulated successfully a larger rainy area, but the simulation for the smaller heavy rainfall centers was slightly inadequate. Comparing with the 24 h observed precipitation (not shown), the precipitation by Expt. RADAR–V is more consistent with the observations. The location of the rainy maximum area simulated by Expt. RADAR–V also is more consistent with the observations. The rainband location and precipitation amount simulated by Expts. RADAR–R and RADAR–RV are similar to the observations, while the simulated maximal rainy areas are not as good as in Expt. RADAR–V. Nevertheless, the results still indicate that the Doppler radar data, including more mesoscale information, are important for the improvement of the quantitative precipitation forecast. In order to get a quantitative verification, equitable threat

score (ETS) and root-mean-square error (RMSE) of the simulated accumulative precipitation from 1200 UTC July 4 to 1200 UTC July 5 have been calculated (not shown), and it is found that Expt. RADAR–V gives the best simulation. Therefore, the simulation result indicates that the radar radial wind produced better simulations than that from radar reflectivity. However, the present result is only from a single example, and more cases should be collected to test and analyze further.

5. The structure and mechanism of MCV by simulation

On the basis of the verification in previous section, the simulation results of Expt. RADAR–V will be used to analyze the formation and structure of the MCV. The structural analysis uses the simulation of the 12-km grid distance, and the vorticity calculation is for

the results of the 4-km grid distance.

5.1 The evolution of the MCV

Figure 8 is the simulated streamline and radar reflectivity at 700 hPa from 1900 UTC 4 July to 0600 UTC 5 July. With the development of the MCS, a closed streamline (vortex) formed at 1700 UTC, with the center located at 32°N, 119°E, but this vortex disappeared gradually (not shown). The severe convection occurred in the southeastern part of the vortex before its dissipation. With the development of the severe convection, a new closed streamline (vortex, located at 32°N, 119°E) occurred in the center of the convection at 2100 UTC 4 July (Fig. 8), which was just the MCV mentioned in section 3. This MCV was maintained for about 10 hours and dissipated after 0500 UTC 5 July. During the development of the MCV, strong reflectivity could be found in the southeastern part of the MCV. The hourly observed precipitation increased gradually from 1900 UTC to 2200 UTC 4 July at Nanjing station (not shown), which means the most severe precipitation occurred before the formation of the MCV. After the formation of the MCV (2100 UTC 4 July), the precipitation had been maintained for several hours. The MCV at 700 hPa gradually dissipated after 0500 UTC 5 July. Compared to the development of the observed MCV (Fig. 5), the initiation time and location of the simulated system are, in many ways, very similar to the observed MCV, although the lifting time of the former was shorter than

the latter.

To understand the vertical distribution of the MCV, the structure of the MCV through the entire troposphere is also diagnosed. It is found that the closed streamline structure only existed in the middle troposphere from 850–600 hPa. The closed streamline occurred first at 850 hPa and 600 hPa at 2300 UTC 4 July, which was two hours later and had weaker intensity and a smaller range than at 700 hPa. At 500 hPa, a short-wave trough was superposed on the vortex in the lower troposphere. In the upper troposphere, a strong divergence circulation could be noticed over the MCV area. According to the above-mentioned analyses, the distinct vortex circulation of the MCV firstly occurred at 700 hPa and extended from 850 hPa to 600 hPa. The most severe precipitation occurred before the formation of the MCV.

The development of the MCV is the process of vorticity production, and here the average vorticity in 31°–35°N, 116°–121°E from 1900 UTC 4 to 0400 UTC 5 July is shown in Fig. 9. The averaged positive vorticity extended from surface to 400 hPa, with the maximum at 800–700 hPa. The vorticity in the lower-middle troposphere increased gradually from $6 \times 10^{-5} \text{ s}^{-1}$ to $10 \times 10^{-5} \text{ s}^{-1}$ from 1900 UTC to 2300 UTC 4 July (Fig. 9a), and decreased gradually from $10 \times 10^{-5} \text{ s}^{-1}$ to $7 \times 10^{-5} \text{ s}^{-1}$ from 0000 UTC to 0400 UTC 5 July (Fig. 9b). Therefore, according to development of the MCV circulation and intensity of the averaged vorticity, the development of the MCV can be divided

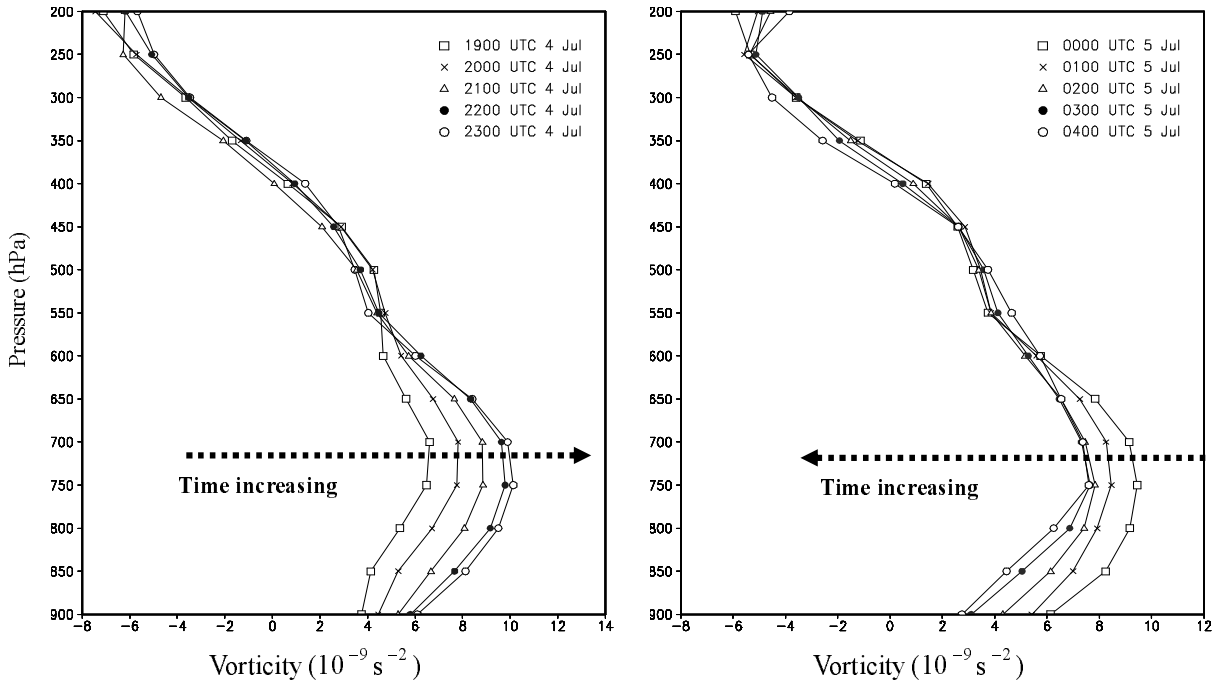


Fig. 9. The vertical distribution of the averaged vorticity (31° – 35° N, 116° – 121° E, MCV, units: $\times 10^{-5} \text{ s}^{-1}$) from 1900 UTC 4 to 0400 UTC 5 July.

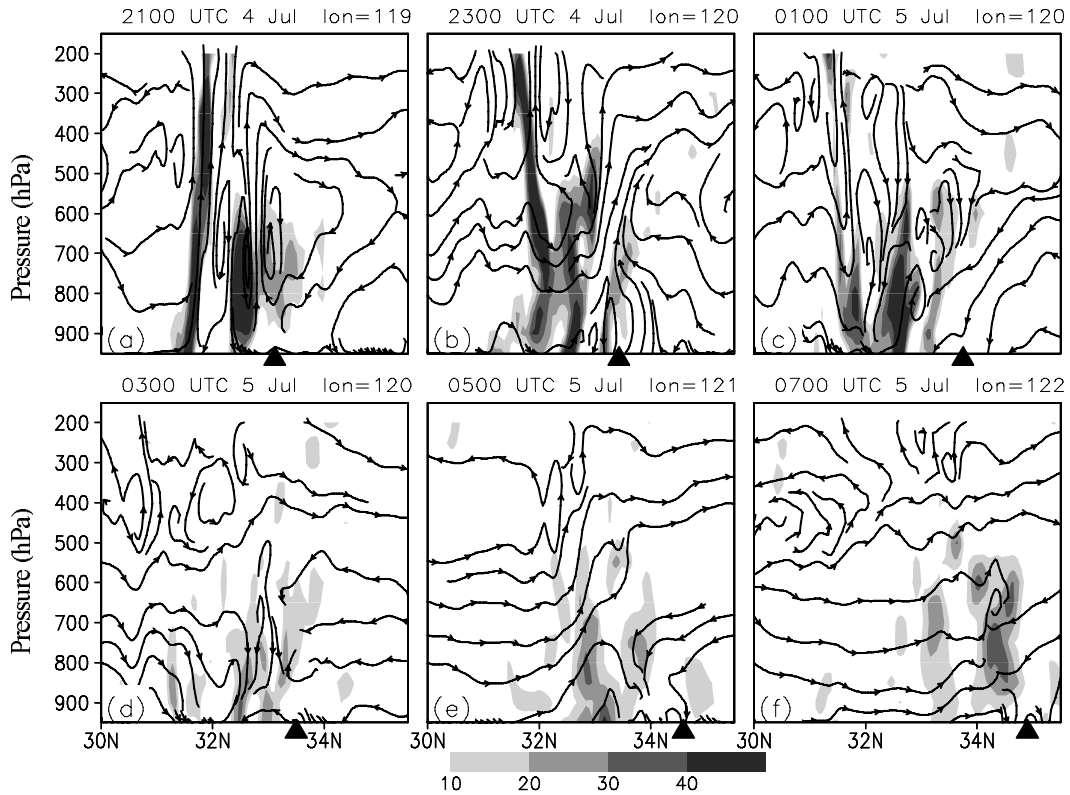


Fig. 10. The vertical cross section of circulation (v ; $w \times 10$, m s^{-1}) and vorticity (shaded, 10^{-5} s^{-1}) along the center of the MCV, where the triangle represents the center of the MCV.

into three stages: initiation stage (before 2300 UTC 4 July), mature stage (2300 UTC 4–0300 UTC 5 July), and dissipating stage (after 0300 UTC 5 July). The structure and vorticity budget of MCV for the three stages will be described in the following section.

5.1.1 The initiation stage (before 2300 UTC 4 July)

At 2100 UTC 4 July, two positive vorticity centers were located at 31.5° and 32.5°N , and the first one extended to the upper troposphere (Fig. 10a). The positive vorticity center corresponded to severe reflectivity greater than 40 dBZ (Fig. 11a). High pseudo equivalent potential temperature and neutral stratification existed in the convection area. The center of the MCV appeared to the north of the positive vorticity and severe reflectivity centers, but the updraft dominated there at this time. At 2300 UTC 4 July, a closed streamline appeared, and the positive vorticity and reflectivity center was relatively weaker than at 2100 UTC 4 July. The updraft still can be found in the center of the MCV (Fig. 10b, Fig. 11b).

5.1.2 The mature stage (2300 UTC 4–0300 UTC 5 July)

At 0100 UTC 4 July, the positive vorticity and reflectivity center were located to the south of the MCV center, and the positive vorticity was far from

the MCV center (Fig. 10c, Fig. 11c). The downdraft motion occurred in the MCV center, and the convection was weaker than that in the initiation stage. At 0300 UTC 4 July, convection disappeared in the MCV center and its surrounding area and the updraft also cannot be found there (Fig. 10d, Fig. 11d). Actually, the convection only exists in the southeastern part of the MCV (Fig. 8).

5.1.3 The dissipating stage (after 0300 UTC 5 July)

After 0500 UTC 4 July, the MCV dissipated gradually. The convection in the southeastern part of the MCV weakened (Fig. 8). During this period, the updraft to the south of the MCV center was also very weak (Figs. 10e, f). The pseudo equivalent potential temperature increase in the lower troposphere indicated stable stratification in the lower troposphere (Figs. 11e, f).

From the above analysis, it is found that the convection occurred in the southeastern part of the MCV. It should be emphasized that in the eastern Asian monsoon region, the LLJ is an important factor for moisture transport and convection development. So, the cross section of wind speed and convection along the eastern part of MCV was analyzed and is shown in Fig. 12. During the initiation stage of the MCV (from 2100 UTC to 2300 UTC 4 July), the LLJ was

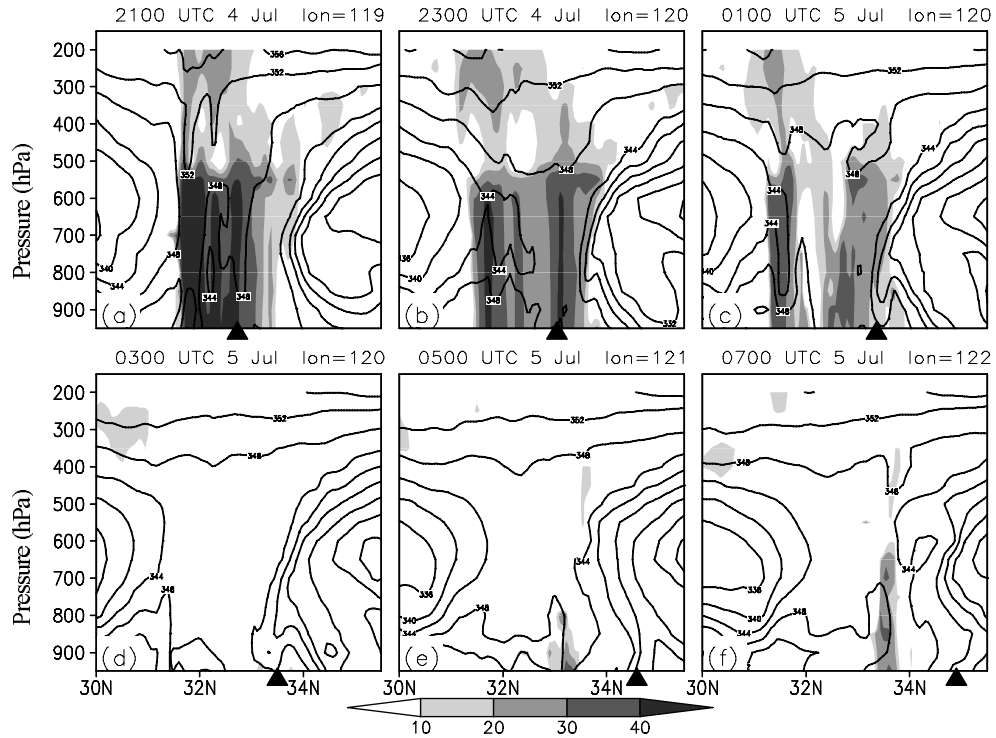


Fig. 11. The vertical cross section of pseudo-potential equivalent temperature (solid line, K) and reflectivity (shaded, dBZ) along the center of the MCV, where the triangle represents the center of the MCV.

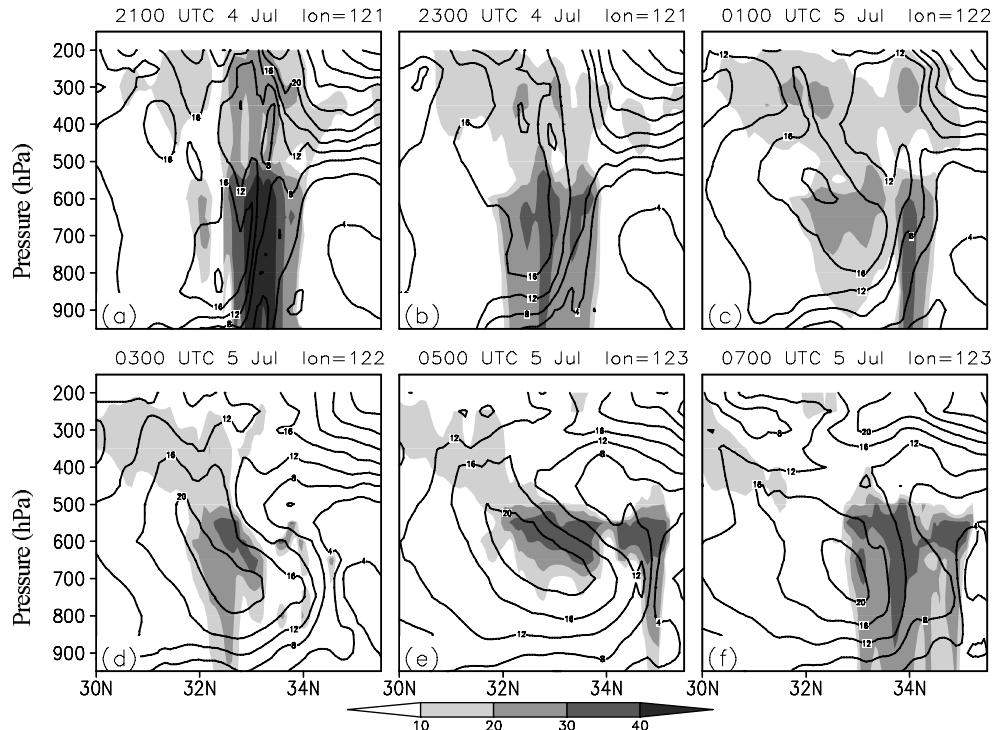


Fig. 12. The vertical cross section of wind speed (solid line, $>12 \text{ m s}^{-1}$) and reflectivity (shaded, dBZ) along the eastern part of the MCV.

stronger than 15 m s^{-1} and extended from 900 hPa to 600 hPa, and the most severe reflectivity just was located to the north of the jet (Figs. 12a, b). During the mature stage of the MCV (from 0100 UTC to 0300 UTC 5 July), the reflectivity was weaker than in the initiation stage of MCV, but the wind speed of the jet increased to 21 m s^{-1} and the isotach of 15 m s^{-1} extended to 300 hPa. New convection areas were developing to the north of the jet center with wind speeds of 21 m s^{-1} (Figs. 12c, d). Even in the dissipating stage, the intensity of the jet was maintained (Fig. 12e), and it weakened after 0700 UTC 5 July (Fig. 12f). In summary, the southerly wind in the eastern part of the MCV intensified after its formation, which may have been favorable to the triggering of new severe convection in southeastern part of the MCV.

5.2 The vorticity budget of MCV

The average vorticity of $31^{\circ}\text{--}35^{\circ}\text{N}$, $116^{\circ}\text{--}121^{\circ}\text{E}$ from the MCV are analyzed and can be divided into different stages, here, the different terms of the vorticity equation were computed to diagnose the sources of vorticity. In pressure coordinates, the model vertical vorticity equation takes the following form:

$$\begin{aligned} \left(\frac{\partial \zeta}{\partial t} \right) = & -\mathbf{V} \cdot \nabla(\zeta + f) - \omega \left(\frac{\partial \zeta}{\partial p} \right) - (\zeta + f) \nabla \cdot \mathbf{V} \\ & + \hat{k} \cdot \left(\frac{\partial \mathbf{V}}{\partial p} \right) + \left[\frac{(F_h + F_v)}{p^*} \right] \zeta, \end{aligned} \quad (1)$$

where \mathbf{V} is horizontal velocity, ζ is the relative vertical vorticity, ω is the vertical velocity in pressure coordinates (x, y, p) , f is the Coriolis parameter, F_h and F_v are the horizontal and vertical momentum transfer coefficients, respectively, and p^* is the pressure difference between the top and bottom of the model atmosphere. The terms on the right side of this equation (from left to right) are horizontal advection, vertical advection, convergence, tilting, and vorticity transfer by friction. The issue of the frictional term presents some difficulty since it is not easy to compute from the model equations, and thus friction can be ignored for the purposes of vorticity budget computations.

The vertical profiles of vorticity show a clear maximum at about the 700-hPa level with a steady decrease in vorticity both above and below this maximum (Fig. 9). The vorticity above 400 hPa was anticyclonic. In order to probe into the details of the formation, each of the first four terms in the vorticity equation [Eq. (1)] were computed hourly at times from the initiation of the vortex to dissipation. The results were plotted in Fig. 13. The figure showed the time evolution of each term from MCV initiation to dissipation. This could provide the some explanation

of the evolution of the MCV. The initial growth in the lower atmosphere appears to result from convergence and tilting, perhaps acting on the planetary vorticity as suggested by Bartels and Maddox (1991). But in the middle atmosphere, the initial sources appeared to come from convergence and vertical advection (Fig. 13a). As the vortex matures, convergence and vertical advection dominated in lower-middle troposphere, but tilting and horizontal advection contributed negatively to the vorticity (Figs. 13b, c). However, at 2300 UTC 4, convergence, and vertical advection are larger than tilting and horizontal advection, the vorticity is increasing (Fig. 13b). At 0100 UTC 5, the vorticity is decreasing while tilting and horizontal advection terms are larger than convergence and vertical advection (Fig. 13c). The features of the vorticity source in the mature stage of the MCV indicate that the vortex would weaken. As the dissipation of the MCV proceeds, vertical advection, and tilting reduce to about zero, and horizontal advection consumes vorticity below 500 hPa. Convergence consumes vorticity below 750 hPa and produces vorticity at 750–400 hPa. In summary, the MCV appeared to be initiated by the convergence and the tilting in the lower troposphere convergence and vertical advection in the middle troposphere.

6. Conclusions and discussions

In the present paper, the MCS/MCVs inducing flooding in the HRB from 3 to 5 July 2003, and which moved from the upper to lower reaches of HRB, are studied. Some results are obtained from the observational data analysis and numerical simulation output:

(1) It is revealed that MCVs exist in East Asia during the mei-yu season and their impact is very significant, particularly with relation to the severe flood caused by a series of secondary convection events related with long-lived MCVs even though MCVs do not appear in every heavy rainfall event.

(2) The synoptic weather pattern analysis shows the easterly propagation of troughs results in the rainy areas moving from upper to lower reaches of HRB. The wide band-shape rainfall area was produced by meso- α scale convective system and MCV.

(3) The numerical simulation results are utilized to diagnose the development process of MCV and its features during three different stages. It is confirmed that the MCV formed during and after the developing of severe MCS. The main closed vortex circulation can be found below 600 hPa, and maximum center is in the middle troposphere. Divergence controls the upper troposphere. The positive vorticity of the MCV extended up to 300 hPa.

(4) The features of the MCV for different stages in

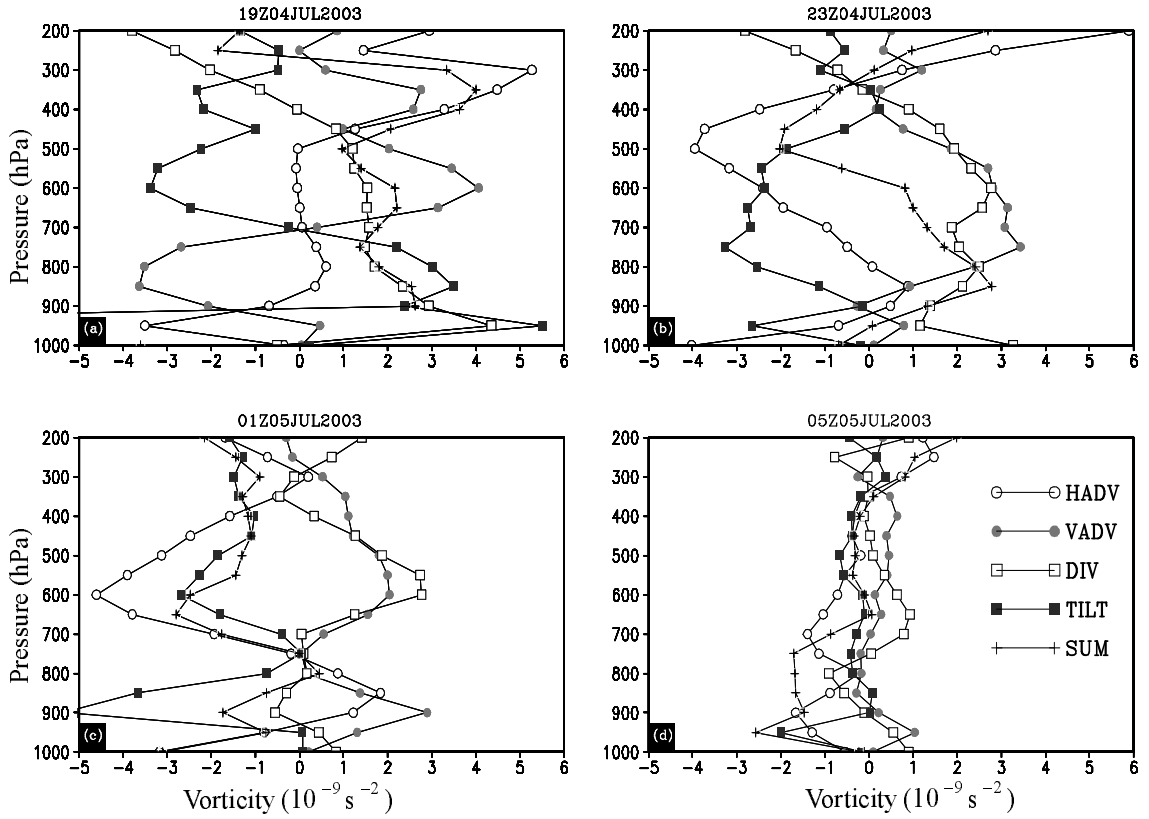


Fig. 13. The vertical distribution of average vorticity of 31° – 35° N, 116° – 121° E, from 4 to 5 July (units: 10^{-9} s^{-2}): (a) 1900 UTC 4; (b) 2300 UTC 4; (c) 0100 UTC 5; (d) 0500 UTC 5 July.

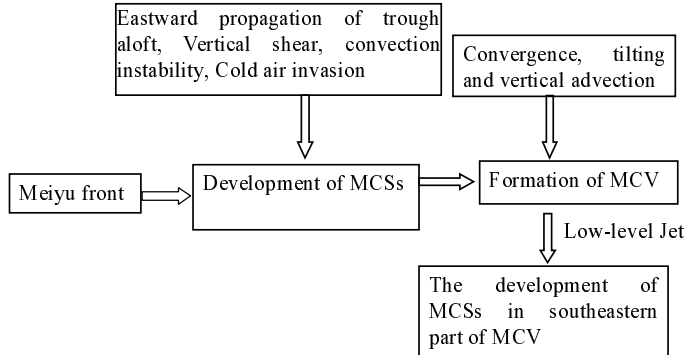


Fig. 14. The conceptual model involving the mei-yu front and embedded MCSs and MCVs.

this case are as follows. During the initiation stage, the MCV occurred to the north of severe convective (the strongest reflectivity and vorticity), and an updraft and neutral stratification were in the MCV center. A downdraft occurred in the center of the MCV and new convection developed in the southeastern part of the MCV during the mature stage. The updraft and convection in the southeastern part of the MCV weakened and stratification became stable gradually during dissipating stage. The above-mentioned mesoscale char-

acteristics, such as the thermodynamic instability and vertical shear, are quite similar to the details of systems in North America, even though the large scale environment conditions are quite different between Asia and North America.

(5) The diagnosis of the vorticity equation during the MCV shows that the convergence and the tilting in the lower troposphere convergence and vertical advection in the middle troposphere were the main vorticity sources in the MCV initiation stage.

(6) A conceptual model between the mei-yu front and the embedded MCS/MCVs has been proposed (Fig. 14). The mei-yu front, a convergence line in the wind field, presents a favorable synoptic condition for the development of MCSs and MCVs. At the same time, the LLJ can transport moisture from the tropical ocean to the mei-yu front region. The weak cold air invasion by eastward propagation of a trough in the middle troposphere may trigger the severe convection under the weak vertical shear and convection instability. During the development of an MCS, an MCV may form in the severe MCS under weak vertical shear and neutral stratification, while vorticity was produced by convergence in the lower troposphere and tilting and vertical advection in the middle troposphere. After the formation of the MCV, the LLJ intensified in the eastern part of the MCV, of which induced initiation of new convection.

Finally, the mentioned-above results are preliminary because the limitation of the spatial and temporal resolution of observational data. Therefore, more MCV cases and high resolution observational data should be collected to study the MCVs along the mei-yu front. In addition, the radar network is not yet completely in China, so only Hefei radar data is utilized. The area covered by the radar in Hefei is limited and could not detect all of the rainy areas. Thus, the initiation fields for the simulation may not be perfect.

Acknowledgements. The authors are grateful to the two anonymous reviewers for their helpful comments. This study was supported by the project of State Key Laboratory of Severe Weather, Chinese Academy of Meteorological Sciences (No. 2009LASW-A03) and the National Natural Science Foundation of China under Grants Nos. 40875021 and 40930951. The Doppler radar data from Hefei station were provided by Dr. ZHOU Haiguang, Chinese Meteorological Academy of Sciences.

REFERENCES

- Bartels, D. L., and R. A. Maddox, 1991: Midlevel cyclonic vortices generated by mesoscale convective systems. *Mon. Wea. Rev.*, **119**, 104–118.
- Bei, N. F., S. X. Zhao, and S. T. Gao, 2002: Numerical simulation of a heavy rainfall event in China during July 1998. *Meteor. Atmos. Phys.*, **80**, 153–164.
- Chen, F., and J. Dudhia, 2001: Coupling an advanced land surface–hydrology model with the Penn State–NCAR MM5 modeling system. Part I: Model implementation and sensitivity. *Mon. Wea. Rev.*, **129**, 569–585.
- Davis, C., and Coauthors, 2004: The Bow Echo and MCV Experiment: Observations and opportunities. *Bull. Amer. Meteor. Soc.*, **85**, 1075–1093.
- Davis, C. A., and S. B. Trier, 2007: Mesoscale convective vortices observed during BAMEX. Part I: Kinematic and thermodynamic Structure. *Mon. Wea. Rev.*, **135**, 2029–2049.
- Ding, Y. H., 1993: *Study on the Lasting Heavy Rainfalls over the Yangtze-Huaihe River Basin in 1991*. Beijing, Chinese Meteorological Press, 255pp. (in Chinese)
- Dudhia, J., 1989: Numerical study of convection observed during the winter monsoon experiment using a mesoscale two-dimensional model. *J. Atmos. Sci.*, **46**, 3077–3107.
- Fritsch, J. M., J. D. Murphy, and J. S. Kain, 1994: Warm core vortex amplification over land. *J. Atmos. Sci.*, **51**, 1780–1807.
- Johnston, E. C., 1981: Mesoscale vorticity centers induced by mesoscale convective complexes. M.S. thesis, Dept. of Meteorology, University of Wisconsin—Madison, 54pp. [Available from University of Wisconsin—Madison, 1225 W. Dayton St., Madison, WI 53706–1695.]
- Johnson, R. H., S. Chen, and J. J. Toth, 1989: Circulations associated with a mature-to-decaying mid-latitude mesoscale convective system. Part I: Surface features—Heat bursts and mesolow development. *Mon. Wea. Rev.*, **117**, 942–959.
- Jorgensen, D. P., and B. F. Smull, 1993: Mesovortex circulations seen by airborne Doppler radar within a bow-echo mesoscale convective system. *Bull. Amer. Meteor. Soc.*, **74**, 2146–2157.
- Kain, J. S., and J. M. Fritsch, 1992: The role of convective “trigger function” in numerical forecasts of mesoscale convective systems. *Meteor. Atmos. Phys.*, **49**, 93–106.
- Kain, J. S., and J. M. Fritsch, 1998: Multiscale convective overturning in mesoscale convective systems: Reconciling observations, simulations, and theory. *Mon. Wea. Rev.*, **126**, 2254–2273.
- Kato, K., 1985: On the Abrupt Change in the Structure of the Baiu Front Over the China Continent in Late May of 1979. *J. Meteor. Soc. Japan*, **63**, 20–36.
- Leary, C. A., and E. N. Rappaport, 1987: The life cycle and internal structure of a mesoscale convective complex. *Mon. Wea. Rev.*, **115**, 1503–1527.
- Lin, Y.-L., R. D. Farley, and H. D. Orville, 1983: Bulk parameterization of the snow field in a cloud model. *J. Clim. Appl. Meteor.*, **22**, 1065–1092.
- Ninomiya, K., 2000: Large- and meso-a-scale characteristics of Meiyu-Baiu front associated with intense rainfalls in 1–10 July 1991. *J. Meteor. Soc. Japan*, **78**, 141–157.
- Ninomiya, K., and T. A. Kiyama, 1974: Band structure of meso-scale echo clusters associated with low-level jet stream. *J. Meteor. Soc. Japan*, **52**, 300–313.
- Ninomiya, K., and H. Muraki, 1986: Large-scale circulations over East Asia during Baiu period of 1979. *J. Meteor. Soc. Japan*, **64**, 409–429.
- Noh, Y., W. G. Cheon, S.-Y. Hong, and S. Raasch, 2003: Improvement of the K-profile model for the planetary boundary layer based on large eddy simulation data.

- Bound. Layer Meteor.*, **107**, 401–427.
- Skamarock, W. C., M. L. Weisman, and J. B. Klemp, 1994: Three-dimensional evolution of simulated long-lived squall lines. *J. Atmos. Sci.*, **51**, 2563–2584.
- Skamarock, W. C., J. B. Klemp, J. Dudhia, D. O. Gill, D. M. Barker, W. Wang, and J. G. Powers, 2005: A Description of the Advanced Research WRF Version 2. NCAR Technical Note TN-468+STR, 88pp.
- Smull, B. F., and R. A. Houze Jr., 1985: A midlatitude squall line with a trailing region of stratiform rain: Radar and satellite observations. *Mon. Wea. Rev.*, **113**, 117–133.
- Sun, J. H., X. L. Zhang, L. L. Qi, G. Y. Zhang, S. X. Zhao, and S. Y. Tao, 2004: A study on vortex and its mesoscale convective system during China Heavy Rainfall Experiment and Study in 2002. *Chinese J. Atmos. Sci.*, **28**(5), 675–691. (in Chinese)
- Sun, J. H., X. L. Zhang, L. L. Qi, and S. X. Zhao, 2005: An analysis of a meso- β system in a Mei-yu front using the intensive observation data during CHeRES 2002. *Adv. Atmos. Sci.*, **22**(2), 278–289.
- Tao, S. Y., 1980: *Heavy Rainfalls in China*. Science Press, Beijing, 1–225. (in Chinese)
- Trier, S. B., C. A. Davis, and J. D. Tuttle, 2000: Long-lived mesoconvective vortices and their environment. Part I: Observations from the central United States during the 1998 warm season. *Mon. Wea. Rev.*, **128**, 3376–3395.
- Weisman, M. L., and C. A. Davis, 1998: Mechanisms for the generation of mesoscale vortices within quasi-linear convective systems. *J. Atmos. Sci.*, **55**, 2603–2622.
- Xue, M., D.-H. Wang, J.-D. Gao, K. Brewster, and K. K. Droegemeire, 2003: The advanced regional prediction system (ARPS), storm-scale numerical weather prediction and data assimilation. *Meteor. Atmos. Phys.*, **82**, 139–170.
- Zhang, D. L., and J. M. Fritsch, 1988a: Numerical sensitivity experiments of varying model physics on structure, evolution and dynamics of two mesoscale convective systems. *J. Atmos. Sci.*, **45**, 261–293.
- Zhang, D. L., and J. M. Fritsch, 1988b: A numerical investigation of a convectively generated, inertially stable, extratropical warm-core mesovortex over land. Part I: Structure and evolution. *Mon. Wea. Rev.*, **116**, 2660–2687.
- Zhang, J., 1999: Moisture and diabatic initialization based on radar and satellite observation. Ph.D. dissertation, University of Oklahoma, 194pp. [Available from School of Meteorology, University of Oklahoma, Norman OK 73019.]
- Zhang, Q. Y., H. J. Wang, Z. H. Lin, J. H. Sun, X. L. Zhang, and J. Wei, 2004 : *The Mechanism of Abnormal Weather and Climate in China—2003*. China Meteorological Press, Beijing, 170pp. (in Chinese)
- Zhao, S. X., Z. Y. Tao, J. H. Sun, and N. F. Bei, 2004: *Study on Mechanism of Formation and Development of Heavy Rainfalls on Meiyu Front in Yangtze River* (In Chinese). China Meteorological Press, Beijing, 282pp. (in Chinese)